A communication channel model for information transmission in the blowfly photoreceptor

Pamela A. Abshire, Andreas G. Andreou *

Department of Electrical and Computer Engineering, The Johns Hopkins University, 3400 N. Charles St., Baltimore, MD 21218, USA

Abstract

Biological photoreceptors transduce and communicate information about visual stimuli to other neurons through a series of signal transformations among physical states such as concentration of a chemical species, current, or the number of open ion channels. We present a communication channel model to quantify the transmission and degradation of visual information in the blowfly photoreceptor cell. The model is a cascade of linear transfer functions and noise sources that are derived from fundamental principles whenever possible, and whose parameters are estimated from physiological data. We employ the model to calculate the information capacity of blowfly phototransduction; our results compare favorably with estimates of the capacity derived from experimental measurements by de Ruyter van Steveninck and Laughlin (Nature 379 (1996) 642–645) and Juusola (J. Gen. Physiol. 104 (1994) 593–621). The model predicts that photon shot noise and ion channel noise are the dominant noise sources that limits information transmission in the blowfly photoreceptor. © 2001 Elsevier Science Ireland Ltd. All rights reserved.

Keywords: Information theory; Channel capacity; Biophysical model; Mathematical model; Blowfly; Photoreceptor

1. Information capacity and the blowfly photoreceptor

Information capacity is a fundamental and quantitative bound on the ability of a physical system to communicate information (Shannon, 1948). The channel capacity of a system corrupted by Gaussian noise is given, in bits per s, by:

$$C = W \log_2 \left(1 + \frac{P}{N}\right)$$

where the channel has noise power N, and the signal has bandwidth W and average power P. This capacity is attained using a signal of Gaussian amplitude distribution. For colored noise, the capacity is (Shannon, 1949):

$$C = \max_{S(f):\sigma_s^2 \le P} \int_0^\infty \log_2 \left(1 + \frac{S(f)}{N(f)}\right) df \qquad (1)$$

where $S(f)$ and $N(f)$ are the power spectral densities of signal and noise, and the optimization

* Corresponding author. Tel.: +1-410-516-8361; fax: +1-410-516-8313.

E-mail address: agalab@olympus.ece.jhu.edu (A.G. Andreou).

is over all signals with variance less than or equal to P.

The signal that maximizes the capacity can be found using the water-filling analogy; the basic idea is that signal energy is concentrated at frequencies where noise is low (Cover and Thomas, 1991). The capacity depends only on the physical properties of the channel, such as bandwidth, noise, and constraints on the signal values; it does not depend on the specific details of any particular task for which the channel may be used. Although it is straightforward to define task-dependent measures of performance, it is appealing to study the maximum information rate, or channel capacity, especially for peripheral sensory systems that are used for many different tasks.

de Ruyter van Steveninck and Laughlin (1996) determined the channel capacity of blowfly photoreceptors. They considered the photoreceptor cell as a whole — a 'black box' — and performed input–output measurements. From the experimental transfer functions and output noise, they calculated the channel capacity. Whereas maximum information rate provides a practical and fundamental bound for the photoreceptor's ability to communicate information, it provides no insights about the factors that limit information transmission. To determine these limiting factors, the 'black box' model for the neuron must be decomposed into its elementary components so that the effects of individual noise sources and inherent bandwidth limitations can be quantified.

We present a communication channel model to quantify the transmission of visual information in the blowfly photoreceptor cell. Our model incorporates all physical transformations from photons entering the compound eye to voltage across the photoreceptor membrane at the synaptic terminal. We describe blowfly phototransduction at a sufficiently detailed level to account for noise sources and bandwidth limitations according to known biophysics, while maintaining a practical approach towards estimating parameters of the model from the available data. Preliminary results from this work were reported in Abshire and Andreou (1998, 1999a,b, 2000a,b).

2. A communication channel model of the blowfly photoreceptor

Blowfly photoreceptors respond to intensity changes with analog changes in their membrane potential. In this investigation, we focus on the photoreceptors R1-6 of *Calliphora vicina* that project to large monopolar cells in the lamina. The blowfly receives behaviorally relevant information from light that is reflected or emitted from objects in the environment. Photons are guided through the optics of the compound eye to the photoreceptors. Absorption of photons activates photosensitive pigments in the photoreceptor cells. The activated pigments trigger a cascade of biochemical reactions that produce 'messenger' molecules. These messengers cause light-gated ion channels in the photoreceptor membrane to open. The open channels provide a membrane conductance that allows an ionic current to flow, changing the membrane voltage. The voltage changes propagate down a short axon to the synaptic terminal in the lamina. In the discussion that follows, we investigate the temporal signals transduced through a single photoreceptor, ignoring spectral, polarization, and spatial aspects of information flow in the system.

Information in the photoreceptor is represented by many different physical structures as the signal is transformed between different physical degrees of freedom: photons, conformational states of proteins, concentrations of chemical messengers, current, and voltage. The overall function of a single photoreceptor is to transfer a message about the world from the light-transducing segment to the axon terminal that synapses onto the large monopolar cell. We model the transformations in the blowfly photoreceptor as a cascade of communication channels that have bandwidth limitations. Each of these transformations is associated with changes in the signal itself and with the introduction of noise. This begins even before transduction, as the arrival times of the photons are randomly distributed. Other sources of noise include the thermal activation of rhodopsin, the stochastic nature of channel transitions, and thermal noise resulting from membrane impedance.
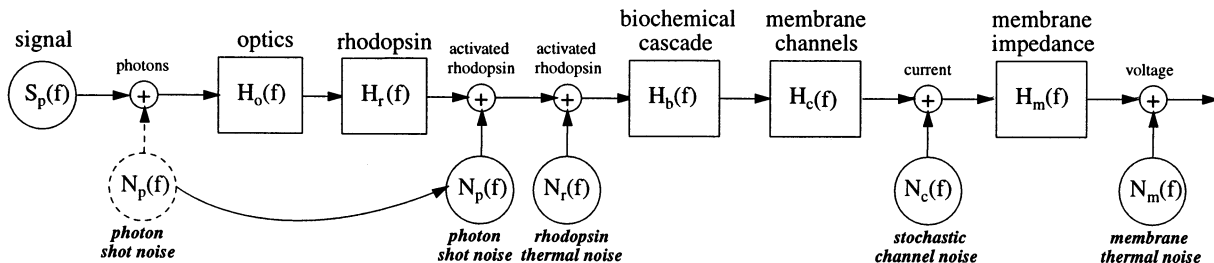
Fig. 1. A communication channel model of the blowfly photoreceptor, showing the transformations corresponding to optics, rhodopsin, biochemical cascade, membrane channels, and membrane impedance and the noise sources corresponding to photon shot noise, rhodopsin thermal noise, stochastic channel noise, and thermal noise due to the membrane impedance.

The model is depicted in Fig. 1, and is mathematically described by Eqs. (2) and (3) below. The signal power $S_n(f)$ at any stage n is transformed through a cascade of linear filters $H_i(f)$. The noise power $N_n(f)$ is the summed power of m independent, additive noise sources $N_j(f)$ that are also transformed by cascades of linear filters. Explicitly, the signal and noise at stage n are given by:

$$S_n(f) = \prod_{i=1}^{n} |H_i(f)|^2 S_p(f) \qquad (2)$$

$$N_n(f) = \sum_{j=1}^{m} \prod_{i=k_j}^{n} |H_i(f)|^2 N_j(f) \qquad (3)$$

where $S_p(f)$ is the power spectral density of the input signal and the noise from independent source j enters at stage k_j.

The input to the system is the light reaching the photoreceptor as a function of time. The output of the system is the membrane voltage at the axon terminal of the photoreceptor. The mean intensity of the incident light determines an operating point, and we employ transfer functions $H_i(f)$, which are linearized about the operating point. While the cells under study exhibit nonlinearity at very low light levels or for large signals (French et al., 1993; Juusola, 1993), they have been studied extensively as linear systems (Leutscher-Hazelhoff and Kuiper, 1964; Eckert and Bishop, 1975; French and Järvilehto, 1978), and their linear properties are well documented in the literature (Juusola et al., 1994, 1995). Modeling the transfer functions $H_i(f)$ as linear systems is accurate when

the variance of the signal is sufficiently small so that the operating point remains fixed. This requirement is satisfied for the stimulation protocols in the experimental studies of de Ruyter van Steveninck and Laughlin (1996), Juusola et al. (1994) and Juusola et al. (1995).

We assume that each of the noise sources $N_j(f)$ contributes independent, additive noise. The transfer functions and noise sources are modeled from first principles when possible and phenomenologically otherwise. Throughout this paper, all spectra are considered to be single-sided, with frequencies ranging from 0 to ∞; for real signals a single-sided spectrum has twice the magnitude of its corresponding double-sided power spectrum. With a communication channel model and its relation to the structure established, we proceed to describe the individual stages in the model, both qualitatively and quantitatively.

2.1. Photons: $S_p(f)$ and $N_p(f)$

Light is a stream of randomly emitted photons. The number of photons observed in any fixed time interval will vary about some average value. This variation can be thought of as 'noise' superimposed on a signal, which is the average number of photons. For most light sources, the photon-counting statistics are described by the Poisson distribution. We take the photon noise to be the signal variance induced by photon shot noise. The power spectral density of the photon noise, in units of (photons per s)^2/Hz, is given by

$$N_p(f) = 2I \qquad (4)$$

where I is the average photon arrival rate, and the factor of 2 is introduced because the spectrum is single-sided. We take the input signal to be the rate of photons reaching the eye as a function of time. The signal and its power spectral density $S_p(f)$ are determined by the environment. Many of the experimental investigations of blowfly vision adopt light stimuli that have Gaussian amplitude distributions and flat frequency spectra (Juusola et al., 1994, 1995; de Ruyter van Steveninck and Laughlin, 1996) because they are amenable to estimation of system response properties.

2.2. Optics: $H_o(f)$

Many insects, including flies, possess an intracellular pupil mechanism for gain control at high light intensities. Upon light adaptation, pigment granules migrate into the light path. These granules absorb light and attenuate the flux reaching the photosensitive pigment. In the physiological literature (Juusola et al., 1994, 1995; de Ruyter van Steveninck and Laughlin, 1996), the average intensity I is calibrated at low light intensities, and, therefore, the effective photon arrival rate accounts for optical spread, but not for the pupillary attenuation. We model the optical transfer function as an attenuation constant C_o that takes values between 0 and 1 and depends on the background intensity I:

$$H_o^2(f) = C_o^2(I) \qquad (5)$$

The optical attenuation was determined experimentally by Howard et al. (1987) as a function of background intensity, by comparing responses between normal and white-eyed flies. White-eyed flies lack the pigments responsible for the intracellular pupil. We fit a sigmoidal function to the data in Fig. 4 of Howard et al. (1987), and we use this function to estimate pupillary attenuation for all light levels:

$$C_o(I) = \frac{\exp[p_1(I + p_2)] + p_3}{1 + \exp[p_1(I + p_2)] + p_3}$$

The data and our empirical fit are shown in Fig. 11, and values for the estimated parameters p_1, p_2, and p_3 are given in the Appendix A.

We have also estimated the pupillary attenuation from membrane noise data of Juusola et al. (1994), and this gives somewhat different results; the parameters, procedures, and results are summarized in the Appendix A.

2.3. Rhodopsin: $H_r(f)$ and $N_r(f)$

The photosensitive pigment is rhodopsin, which consists of the chromophore retinal linked to the protein opsin. At low light intensities discrete bumps can be observed in the membrane voltage; each of these bumps results from current flow that follows the absorption of a single photon and resultant isomerization of rhodopsin. Even in the absence of light, photoreceptors exhibit discrete electrical responses which are indistinguishable from single photon absorptions; these dark events are attributed to the spontaneous thermal isomerization of rhodopsin molecules (Birge and Barlow, 1995). The transformation from photons to activated rhodopsin molecules is modeled by the transfer function $H_r(f)$, in units of (Rh*/photon), denoting rhodopsin isomerization per photon, and rhodopsin thermal isomerization is modeled by the noise source $N_r(f)$, in units of $(\text{Rh*/s})^2/$Hz, given by:

$$H_r^2(f) = \eta^2 \qquad (6)$$

$$N_r(f) = 2\lambda_r \qquad (7)$$

We take the quantum efficiency to be $\eta = 1$, and the thermal isomerization rate to be $\lambda_r = 10^{-3} \text{ s}^{-1}$. Any quantum efficiency less than unity is absorbed into the calibration for effective photon rate that was described in Section 2.2. Estimates for the thermal isomerization rate range from 10^{-3} (Birge and Barlow, 1995; Hochstrate and Hamdorf, 1990) to $< 3 \times 10^{-3} \text{ s}^{-1}$ (Lillywhite, 1977).

As described in Section 2.1, photon shot noise is modeled by a Poisson point process. Not all incident photons contribute to the signal; some are absorbed by the pigment granules, and some fail to be absorbed by rhodopsin molecules. These

absorptions and failures cause a random deletion of events in the photon stream that generates another Poisson process with a lower arrival rate (Teich and Saleh, 1982). The effective photon shot noise, taking into account pupillary absorption and quantum efficiency, is given by:

$$N_p(f) = 2I\eta C_o(I) \tag{8}$$

We indicate this correction to the photon shot noise by the dotted lines and transposition of the photon noise source to an effective activated rhodopsin noise shown in Fig. 1.

2.4. Biochemical cascade: $H_b(f)$ and $N_b(f)$

Each activation of a rhodopsin molecule triggers a cascade of biochemical reactions. This cascade ultimately produces molecules that control the properties of light-gated channels in the photoreceptor membrane. Changes in the channel properties translate into changes in the membrane conductance. Since the details of the biochemical cascade in invertebrates remain unknown, our model for the biochemical cascade is phenomenological. We consider the biochemical cascade to be a noiseless impulse response to each activated rhodopsin molecule, a 'bump' in the membrane conductance. This is essentially the adapting bump model developed by Wong and Knight (1980), Wong et al. (1980), and Wong et al. (1982), with the impulse response modeled as a gamma function. The biochemical cascade filters the power spectral density of the visual signal by the transfer function $H_b^2(f)$, with units of (S/ Rh*)^2:

$$H_b^2 = \frac{h_b^2}{[1 + (2\pi f t_b)^2]^{n_b + 1}} \tag{9}$$

We estimate the parameters of the biochemical cascade transfer function from physiological data; the parameters and procedures are summarized in Appendix A.

We do not model any noise sources contributed in the biochemical cascade (i.e. $N_b(f) = 0$).

2.5. Stochastic channels: $H_c(f)$ and $N_c(f)$

The blowfly photoreceptor membrane depolar-

izes in response to light increments, quickly reaching a peak and eventually decaying to a steady state value. This steady state membrane voltage increases with light. The light-gated current is carried primarily by sodium and calcium ions. Potassium current opposes the voltage change induced by the light-gated flow.

Membrane channels are proteins which form pores through the cellular membrane. The pores can allow ions to flow in and out of the cell ('open' state) or prevent that flow ('closed' state). The probability that the light-gated channels are open or closed is modulated by the messenger molecules produced by the biochemical cascade. This physical mechanism transforms conductance into current across the membrane. The transfer function from conductance to membrane current is given by Ohm's law, in units of (V)^2:

$$H_c^2(f) = (V_m - E_L)^2 \tag{10}$$

where V_m is the membrane voltage, and E_L is the reversal potential for the ions that flow through the light-gated channels.

Transitions between the states of a channel are stochastic. The transition probabilities can be modulated by the membrane voltage, as for the potassium channels, or by the presence of a ligand, as for the light-gated channels. Fluctuations in the number of open channels introduce noise in the membrane current. Channel kinetics lead to Lorentzian power spectral densities; for details consult Johnston and Wu (1997) or DeFelice (1981). The model for current noise in a simple channel population with an open and a closed state, time constant τ_c, open probability n_∞, single channel conductance γ_c and N independent channels, is given by:

$$N_c(f) = \frac{4N\gamma_c^2(V_m - E_{ch})^2 n_\infty(1 - n_\infty)\tau_c}{1 + (2\pi\tau_c f)^2} \tag{11}$$

We model the noise contributed by potassium channels and light-gated channels in the blowfly photoreceptor according to Eq. (11), using parameters for channel data reported in Weckström et al. (1991), Reuss et al. (1997), Hardie

and Minke (1993) and Hardie and Minke (1994) and channel activation parameters estimated from our model of membrane impedance and summarized in Appendix A. Noise contributed by the leakage channels is not modeled. More complex behavior, specifically more than one channel type, is suggested for the potassium channels by Weckström et al. (1991) and for the light-gated channels by Reuss et al. (1997), but we utilize the simple model in Eq. (11) because the data available for estimating parameters is limited.

The introduction of channel kinetics implies a dynamical component to the transfer function $H_c(f)$ of Eq. (10), specifically a first-order low pass transfer characteristic with time constant τ_L caused by the light-gated channels. Ideally, this dynamical component should be modeled separately, but such a model would require estimation of the time constant for the light-gated channels as a function of incident intensity. Our review of the literature did not reveal this data, so we absorb the dynamical portion of this transfer characteristic into the biochemical cascade transfer function that was discussed earlier in Section 2.4.

2.6. Membrane impedance: $H_m(f)$ and $N_m(f)$

The current that flows across the membrane in the light-transducing region changes the local voltage that propagates to the axon terminal of the cell. The photoreceptor is an elongated structure, so we employ cable theory to account for the propagation of the signal in the cell. Following van Hateren (1986), we abstract the distributed properties of the cell into three lumped-parameter compartments. Two segments represent the cell body and the third represents the axon, as shown in Fig. 2(a). Each segment is modeled as a two-port network, with axoplasm impedance z_a and membrane impedance z_m (see Fig. 3). The two-port impedances of the cell body are Z_H and Z_V, $2l_b$ is the length of the cell body, and Z_t is the terminal impedance of the axon.

$$Z_H = \frac{\sqrt{z_a z_m} \cosh(\sqrt{z_a/z_m} l_b)}{\sinh(\sqrt{z_a/z_m} l_b)}$$
$$Z_V = \frac{\sqrt{z_a z_m}}{\sqrt{z_a/z_m} \sinh(\sqrt{z_a/z_m} l_b)} \tag{12}$$

The two-port impedances of the axon are computed analogously using the axon length l_a The input impedance is given by $Z_{in} = V_1/I_1$, the transfer impedance from input to synaptic terminal is $Z_{tr} = V_4/I_1$, and the output impedance is $Z_{out} = V_4/I_4$.

The compound eye of the blowfly exhibits neural superposition (Braitenberg, 1967). Six photoreceptors receive light from the same direction, but through different facet lenses, and project to the same column in the lamina. These cells are coupled to their next neighbors by gap junctions at their axon terminals (Shaw, 1984). This anatomical arrangement is modeled by the equivalent circuit shown in Fig. 2(b) (van Hateren, 1986). The six photoreceptors are coupled by impedances R_g representing the gap junctions. The resistance barrier between extracellular space in the lamina and extracellular space in the receptor layer is represented by impedance R_b.

An equivalent circuit model of the membrane impedance z_m in a single compartment is shown in Fig. 3. The membrane model consists of a capacitance C_m, light-gated conductance g_L with reversal potential E_L, leakage conductance g_{leak} with reversal potential E_{leak}, and potassium conductance g_K with reversal potential E_K and dynamical parameters g_n and L_n that model the voltage dependence of the potassium channels. These membrane parameters contribute axoplasm impedance z_a and membrane impedance z_m given by:

$$z_a = \frac{R}{\pi r^2} \tag{13}$$

$$z_m = \frac{1 + 2\pi j f L_n g_n / SA}{g_n + g_m - g_n C_m L_n (2\pi f)^2 + 2\pi j f (C_m + L_n g_n g_m)} \tag{14}$$

$$g_m = g_L + g_{leak} + g_K \tag{15}$$

where r is the compartment radius, R is the axoplasmic resistivity and SA is the surface area of the compartment, per unit length. The surface area per unit length for the axon is $2\pi r_a$, but the cell body surface area is dominated by the microvilli that form the lightguide, so the formula is $2\pi r_b + SA_{rhab}$. Weckström et al. (1992) report evidence suggesting that there may be unique conductance mechanisms in the axon that are absent
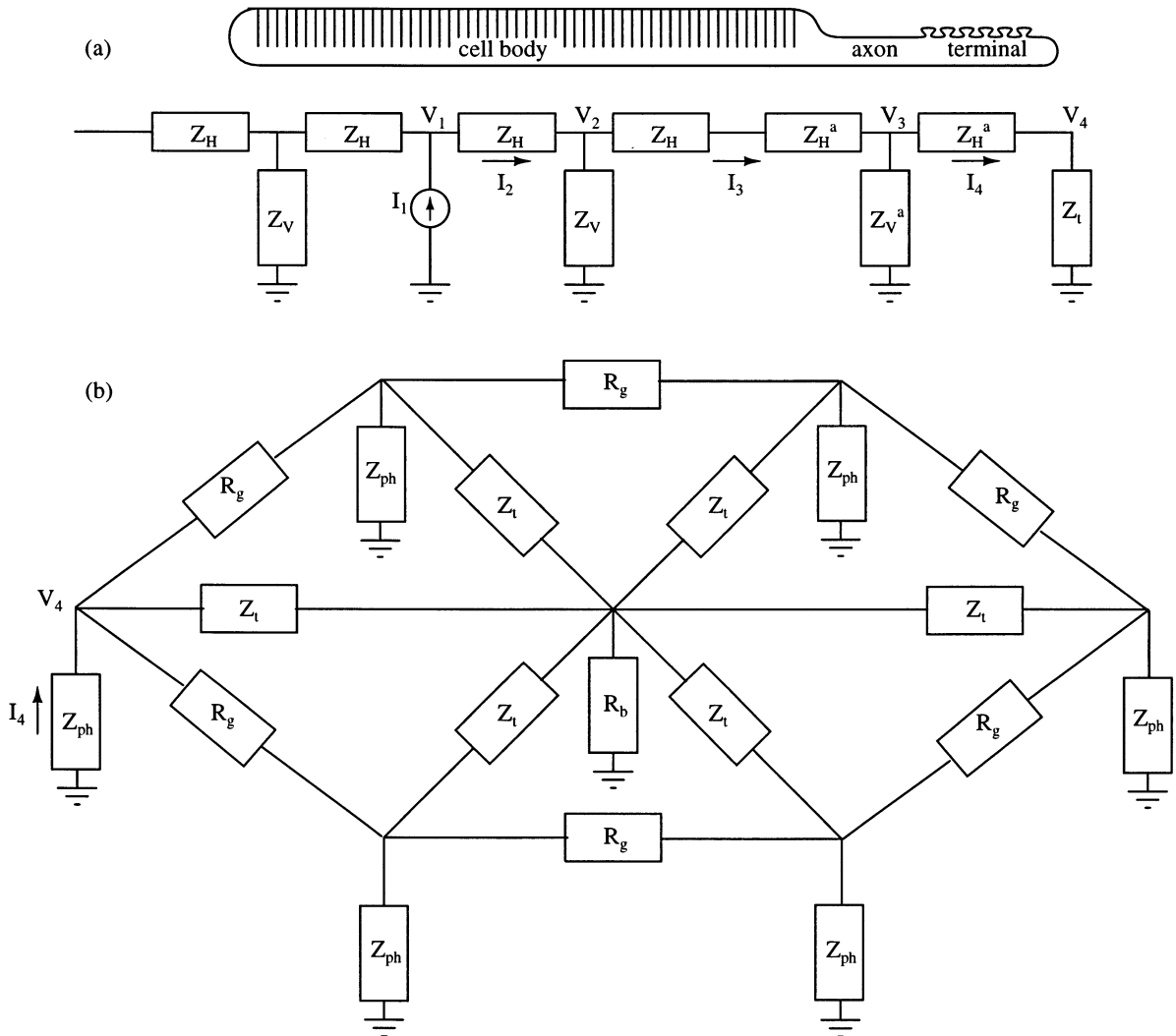
Fig. 2. Cable models for the photoreceptor, after van Hateren (1986). (a) A three compartment model for the photoreceptor, with two compartments corresponding to the cell body and a single compartment corresponding to the axon. (b) An equivalent circuit showing a photoreceptor coupled by gap junctions to its six neighbors in the lamina. The impedance Z_{ph} represents the input impedance of a photoreceptor as seen from its axon.

in the cell body, but these conductances have not been characterized in detail. We use an identical membrane model for the cell body and axon compartments.

We estimate the parameters $g_L(V)$, $g_K(V)$, $g_n(V)$, g_{leak}, $L_n,(V)$, r_b, l_b, SA_{rhab}, and E_{leak} of the membrane model from physiological data; please see Appendix A for brief descriptions of those parameters and procedures.

The signal is transformed from current in the light-transducing segment to voltage at the synaptic terminal by the transfer impedance Z_{tr}. Both signal and noise are filtered by the transfer function $H_m^2(f)$, in units of Ω^2, given by:

$$H_m^2(f) = |Z_{tr}|^2 \tag{16}$$

Thermal equilibrium noise, caused by thermal agitation of electrical charges, provides a funda-
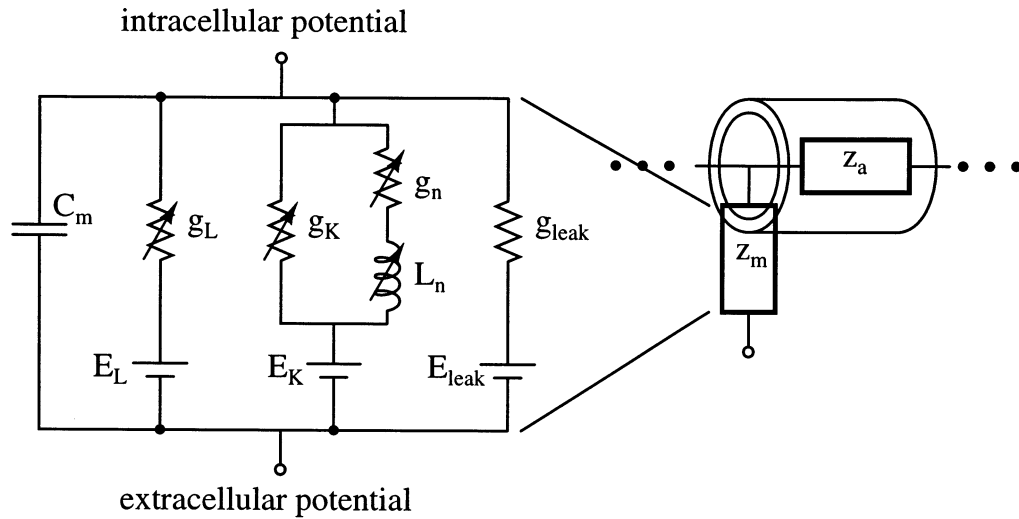
intracellular potential

Fig. 3. Model for photoreceptor membrane impedance incorporating weakly active potassium channels. The sketch on the right shows the membrane impedance in the context of a cable segment.

mental lower limit to noise in any system. An arbitrary impedance $Z(f)$ contributes thermal voltage noise with spectral density $N_V(f) = 4kT\mathrm{Re}[Z(f)]$. Thus the photoreceptor membrane impedance contributes thermal noise, in units of V^2/Hz, given by:

$$N_m(f) = 4kT\mathrm{Re}[Z_{out}(f)] \qquad (17)$$

3. Results and discussion

We employ the model presented in Section 2 to calculate the signal, noise, and capacity at each intermediate stage of the system for various operating points. In Fig. 4, we compare the noise predicted by our model with the noise measured in the membrane voltage. The left panel shows data from Juusola et al. (1994) that represent the noise power spectral density of the photoreceptor membrane voltage, for several background light levels. The right panel shows the prediction of our model at the same light levels. We model the noise at the photoreceptor cell body as the cumulative noise due to photon noise, rhodopsin noise, chan-

nel noise, and thermal noise[1]. While there are obvious quantitative differences between the model and the data, there are striking qualitative similarities. For example, as the background light level increases, the noise level increases at first, then falls again as the light level continues to increase in both model and data. Furthermore, portions of the noise spectra are relatively flat up to some cutoff frequency, and this cutoff frequency increases with light adaptation for both model and data. However, our model does not predict the increase in noise below 5 Hz, which is evident in the experimental data of Juusola et al. (1994) and also in the experimental data of Juusola et al. (1995). This excess noise may be contributed by the gain control mechanism of the intracellular pupil, which is known to have dynamics on this time scale (Hardie, 1979). An alternative explanation for the source of this excess noise is the biochemical cascade, which also shows adaptation on this time scale.

---

[1] Z_{tr} and Z_{out} should be replaced by Z_{in} in Eqs. (16) and (17), respectively, for predictions at the cell body rather than the axon terminal.
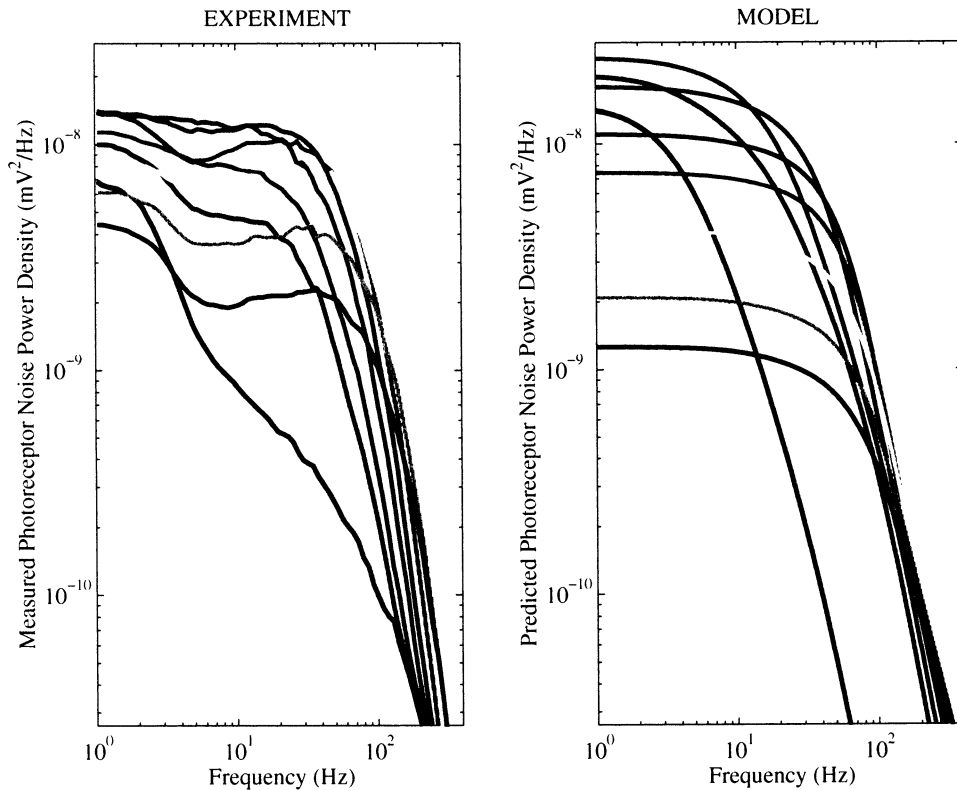
Fig. 4. Photoreceptor membrane voltage noise. The left panel shows data from Juusola et al. (1994), and the right panel shows noise predicted by our model, using parameters estimated from the transfer function data of Juusola et al. (1994) and pupillary attenuation as determined by Howard et al. (1987). The different traces are for different background light levels, color coded so that purple to blue to green to red corresponds to the light levels [dark, 160, 500, 1600, 5000, 16000, 50000, 160000, 500000] effective photons per s.

In Fig. 4, the noise predicted by our model at higher light levels falls below the measured noise. In Appendix A, we describe an alternative method for estimating the pupillary attenuation using the membrane noise data of Juusola et al. (1994). The left panel of Fig. 5 shows the same data from Juusola et al. (1994), and the right panel shows the prediction of our model using the alternative parameters for pupillary attenuation. The alternative prediction of Fig. 5 demonstrates quantitative agreement between modeled and measured noise. This agreement was achieved by estimating the pupillary attenuation as a function of incident intensity. Pupillary attenuation decreases the photon count in any interval and increases the photon noise contribution. Thus, the alternative parame-

ters cause the optical transmission to be more attenuated than the estimates of Howard et al. (1987) and the photon noise to increase at the higher light levels for which the predicted noise was earlier smaller than the measured noise (Fig. 4). We note that the noise data of Juusola et al. (1995) is quantitatively very different from the noise data of Juusola et al. (1994). The noise measured by Juusola et al. (1995) did not agree quantitatively with the noise predicted by our model using parameters estimated from the transfer functions of Juusola et al. (1995). An alternative pupillary attenuation did not improve the results.

By referring the predicted noise shown in Fig. 4 to the input, using the transfer functions presented in Section 2, we compute the information
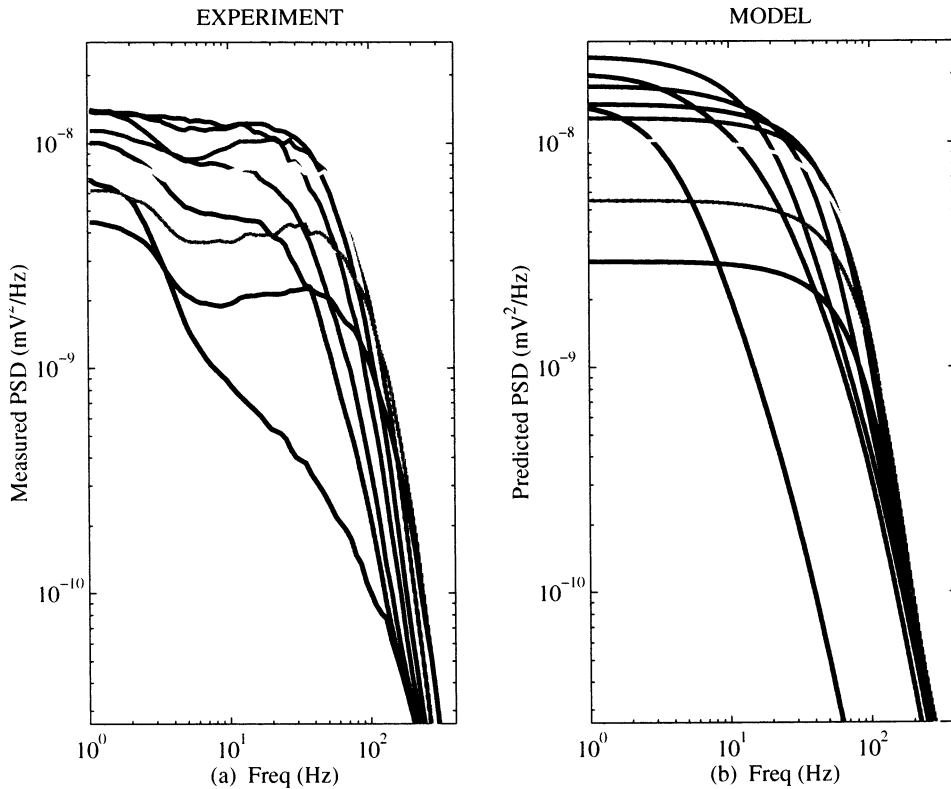
EXPERIMENT   MODEL

Fig. 5. Photoreceptor membrane voltage noise. The left panel shows data from Juusola et al. (1994), and the right panel shows noise predicted by our model, using parameters estimated from the transfer function data of Juusola et al. (1994) and pupillary attenuation estimated from the noise data of Juusola et al. (1994). The different traces are for different background light levels, color coded so that purple to blue to green to red corresponds to the light levels [dark, 160, 500, 1600, 5000, 16000, 50000, 160000, 500000] effective photons per s.

capacity of the blowfly photoreceptor using Eq. (1)[2]. The capacity is plotted in Fig. 6 as a function of incident light intensity. Estimates from de Ruyter van Steveninck and Laughlin (1996) are shown along with the results of the model presented in this paper and the photon shot noise limit. The photon shot noise is computed with and without pupillary attenuation as determined by Howard et al. (1987). The results are indistin-

guishable when plotted; only the photon noise without pupillary attenuation is shown in Fig. 6. The information capacity predicted by our model is computed at the cell body and at the axon terminal. The results of this calculation are indistinguishable when plotted; only the capacity at the cell body is shown, for comparison with the estimates by de Ruyter van Steveninck and Laughlin from measurements at the cell body.

We can obtain an independent estimate of the capacity as a function of background light from data of Juusola et al. (1994). The data shown on the left in Figs. 4 and 5 represents membrane voltage noise from Fig. 5c of Juusola et al. (1994), and data shown in Fig. 10 of the Appendix A, scaled from Fig. 7 of Juusola et al. (1994), repre-

---

[2] Note the implicit assumption that all noise sources are normally distributed, wherease photon shot noise has a Poisson distribution. The Poisson distribution approaches the normal distribution for high mean values, so this assumption does not hold for very low light levels. The approximation is reasonable at the lowest light level considered, 160 effective photon/s.

sents the transfer function from photons to membrane voltage. In Fig. 7, we show the capacity computed from the data of Juusola et al. (1994), along with the prediction of our model for capacity at the cell body using the alternative pupillary attenuation. For comparison, we also show the estimates of capacity from de Ruyter van Steveninck and Laughlin (1996), the prediction of our model from Fig. 6, and the shot noise limit before and after pupillary attenuation using alternative parameters. The capacity computed using the pupillary attenuation from Howard et al. (1987) matches well the estimates of de Ruyter van Steveninck and Laughlin (1996), and the capacity computed using the alternative pupillary attenuation matches the estimates from the data of Juusola et al. (1994). When the model is adjusted to fit the noise data (i.e. using the alternative parameters for pupillary attenuation), the

capacity predicted by the model corresponds closely to the capacity computed from the same data (the circles in Fig. 7).

The channel capacity given by Eq. (1) is an upper bound on the rate of information transmission, assuming that the signal is limited only in average power and the noise is normally distributed. Although these assumptions are not strictly true for the photoreceptor, Eq. (1) closely approximates the actual capacity. Bandwidth limitations alone do not limit information transmission; a bandwidth limitation which affects signal and noise equally does not affect the channel capacity. Capacity can be increased arbitrarily by increasing the signal power; we must specify how the signal power is constrained so that Eq. (1) is meaningful. Experiments in the blowfly usually specify a fixed contrast power σ_c^2, in particular $\sigma_c^2 = 0.1$ in Juusola et al. (1994, 1995) and de
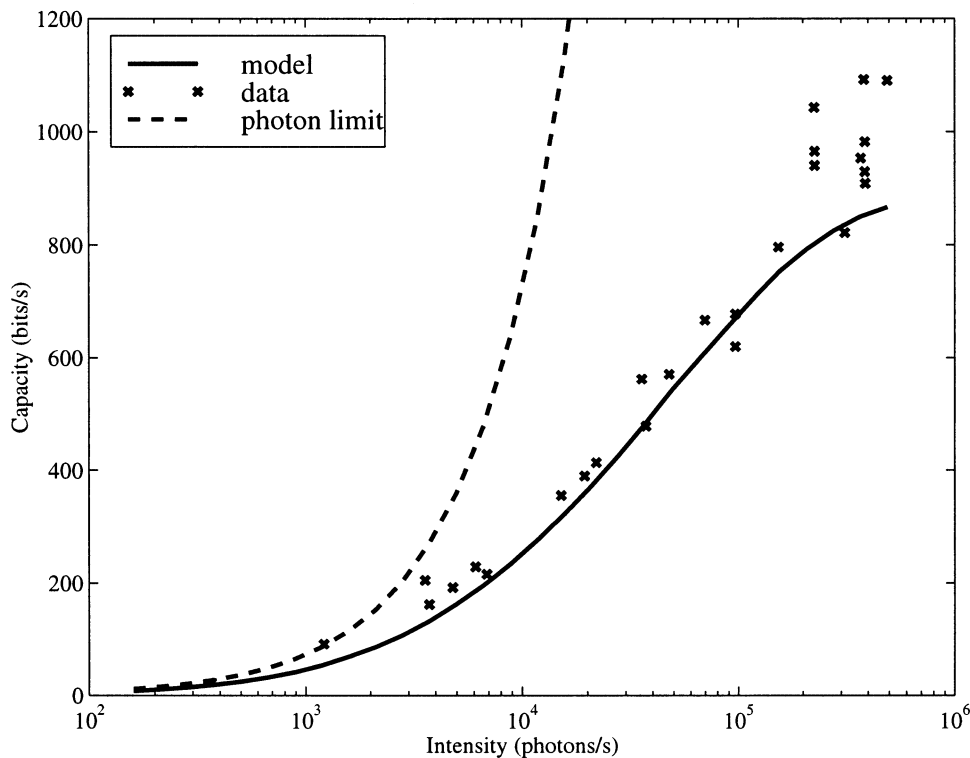

Fig. 6. Information capacity computed from our model and estimated from experimental data, as a function of background light intensity. 'x's are experimental estimates by de Ruyter van Steveninck and Laughlin (1996), the solid line is the result from our model, and the dashed line is the photon shot noise limit before pupillary attenuation.
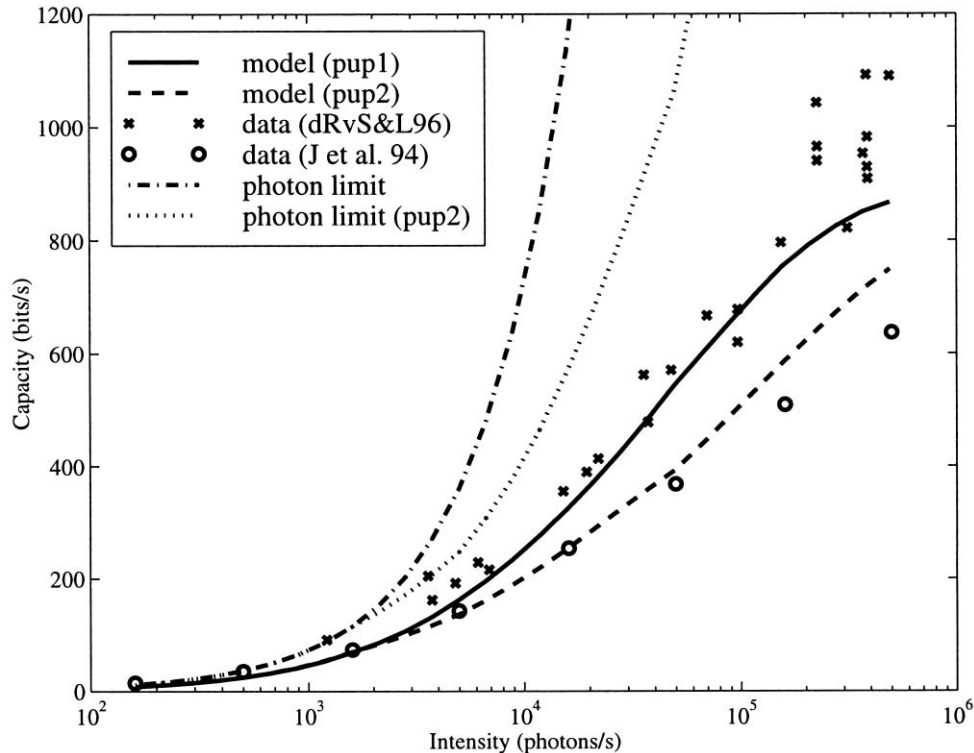
Fig. 7. Information capacity computed from our model and estimated from experimental data as a function of background light intensity. 'x's are estimates from de Ruyter van Steveninck and Laughlin (1996), and 'o's are estimates computed from the data of Juusola et al. (1994). The solid and dashed lines are the results from our model, and the dash-dotted and dotted lines are the photon shot noise limit, before and after pupillary attenuation estimated from the noise data of Juusola et al. (1994), respectively. The upper result from the model (solid line) uses the pupillary attenuation as determined by Howard et al. (1987), and the lower result (dashed line) uses the pupillary attenuation as estimated from the noise data of Juusola et al. (1994).

Ruyter van Steveninck and Laughlin (1996). In this paper, we adopt the convention of fixed contrast power $\sigma_c^2 = 0.1$, where contrast is defined as the normalized intensity ($\sigma_c^2 = \sigma_I^2/I^2$), so that our theoretical results are comparable to published experimental results.

The detailed model presented in this paper enables us to predict the relative contributions of the noise sources that ultimately limit the rate of information transmission. Fig. 8 shows the fraction of total output-referred noise, i.e. voltage noise power at the photoreceptor axon, which is contributed by each of the noise sources in the model, as a function of background intensity. The dominant noise sources are photon shot noise and the stochastic channel noise over all background intensities. At the cell body, thermal noise is insignificant at all background intensities. At the axon terminal, thermal noise becomes significant at higher light intensities, however, its contributions are concentrated at higher frequencies, which are unlikely to be relevant physiologically or behaviorally.

We have analyzed information processing in the blowfly photoreceptor, by modeling it as a communication system constrained by the physical components from which it is constructed, from photons to rhodopsin to biochemistry to membrane currents to membrane voltage. The physical instantiation of each channel determines the noise, bandwidth and amplitude constraints for the signals. Such detailed analysis relates function to structure in a fundamental and quantitative manner.
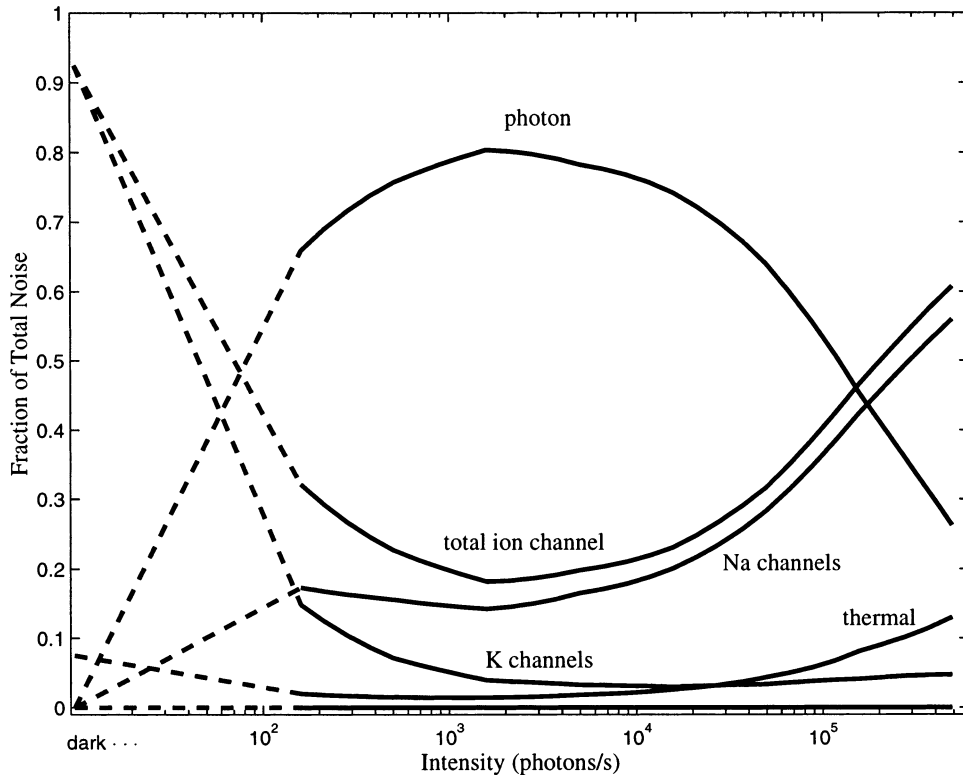
Fig. 8. Fraction of the total output noise variance at the photoreceptor axon contributed by each independent noise source, as a function of background light. The photon shot noise and stochastic channel noise are dominant at all background light levels.

The model presented in this paper integrates a great deal of earlier disparate knowledge about blowfly phototransduction. Parts of the model were developed by earlier authors, for example the adapting bump model of Wong et al. (1980) and the cable model of van Hateren (1986). In this work, we integrate knowledge in a way consistent with both the underlying biophysics and an information theoretic framework. There are many assumptions and simplifications in our model, and perhaps inconsistencies in the data, but nonetheless our results are encouraging. The remarkable outcome is not the perfection of any individual fit to the experimental data, but rather, that when the system is considered as a whole, with model parameters estimated from available data, the system's performance is predicted well without introducing free parameters.

Detailed analysis of a complex system inevitably requires the estimation of many parameters. To maintain clarity in our description of the model, we defer discussion about parameter estimation to Appendix A. For the model presented in this paper, we estimated parameters from data reported in many sources, tabulated in Table 1 of Appendix A. It is not reasonable to expect that all of these different measurements, by different experimenters using different flies and sometimes different species, will represent the properties of any single cell. This is not a fundamental limitation in our approach but rather a practical limitation. We believe that our formulation is very general, and anticipate that, if the appropriate data were available, our model would describe it well.

Table 1
Descriptions, values, and citations for published data.

Description	Value(s)	Reference
Rhodopsin thermal isomerization rate	$\approx 10^{-11}$ events/rhodopsin per s	Birge and Barlow (1995)
Rhodopsin content for *Calliphora* photoreceptor	$\approx 10^{8}$ rhodopsin molecules	Hochstrate and Hamdorf, 1990
Spontaneous isomerization rate in a locust photoreceptor	<1 per 6 min	Lillywhite (1977)
Parameters for voltage-activated K channels in photoreceptor membrane	$V_r = -60$ mV, $E_K = -85$ mV, $\gamma_K = 20$ pS, $N_K = 10^4$, activation threshold for K channels ≈ -75 mV	Weckström et al. (1991)
Channel open time for light-gated channels	$\tau_1 = 1.8$ ms	Hardie and Minke (1994)
Reversal potential for light-gated channels	$E_L = 10$ mV	Hardie and Minke (1993)
Single channel conductance for light-gated channels	$\gamma_L = 17$ pS	Reuss et al. (1997)
Photoreceptor membrane parameters	$R = 1.0$ Ωm, $C_m = 1$ μF/cm^2, $C_t = 2.2$ pF, $R_t = 100$ MΩ, $r_a = 2$ μm, $l_a = 35$ μm, $R_g = 25$ MΩ, $R_b = 2$ MΩ, $R_m = 8$ KΩcm^2, $r_b = 2.5$ μm, $l_b = 125$ μm, and $SA_{rhab} = 40$ μm	van Hateren (1986)
Photoreceptor transfer function at different light levels (photon per s → membrane voltage)	Fig. 7	Juusola et al. (1994)
Photoreceptor membrane voltage noise at different adapting backgrounds	Fig. 5c	Juusola et al. (1994)
Steady state voltage V_m for photoreceptor membrane at different adapting backgrounds	Fig. 4a	Juusola et al. (1994)
Input impedance of dark-adapted photoreceptor membrane $\lvert Z_{in}(f)\rvert$ at different fixed voltages	Fig. 4b	Juusola and Weckström (1993)
Estimated capacity of photoreceptor and LMC at different adapting backgrounds	Fig. 3	de Ruyter van Steveninck and Laughlin (1996)
Pupillary attenuation for photoreceptor	Fig. 4	Howard et al. (1987)
Photoreceptor transfer function at different adapting backgrounds (photon per s → membrane voltage)	Fig. 7A	Juusola et al. (1995)
Photoreceptor membrane voltage noise at different adapting backgrounds	Fig. 11A	Juusola et al. (1995)

4. Conclusions

In the fifty years since Shannon's first probabilistic formulation of information theory, its concepts and tools have been employed many times to better understand neural systems from a functional perspective. Attneave (1954) and Barlow (1961) introduced the idea that representation in neural systems is guided by coding principles from information theory. Since then, information theoretic principles have motivated both theoretical and experimental studies of neural coding. The early qualitative observations about neural representation have been expanded and developed more rigorously (Atick, 1992; Linsker, 1986; Laughlin, 1994). Other studies employ abstract mathematical models to investigate coding strategies for single spiking neurons (MacKay and McCulloch, 1952; Stein, 1967; Levy and Baxter, 1996). A rich literature has emerged using measurements from neural systems to quantify information rate under specific experimental conditions (Eckhorn and Pöpel, 1974; Theunissen and Miller, 1991; Rieke et al., 1997; Buračas et

al., 1998). These quantitative results contribute to understanding coding strategies, neural computation, and the reliability of neural signals.

To elucidate the principles of information processing in physical systems, we must relate the functional understanding gained through such information theoretic studies to the physical properties of the systems under study. We believe that it is important to understand neural systems in terms of fundamental and practical noise limitations at the cellular level, because noise limitations ultimately set the performance limits that determine behavior. The physical limits to behavior were discussed by Bialek (1987), and more recently, Manwani and Koch (1999) have addressed fundamental noise limitations in neural systems from a biophysical perspective.

Earlier information theoretic approaches have left important questions unanswered: 'how does information theory relate to biophysics of the real neuron?'; and more specifically, 'how do quantitative information theoretic measures relate to the limitations of the physical structures?' The work presented in this paper is a first step towards providing rigorous answers to these questions.
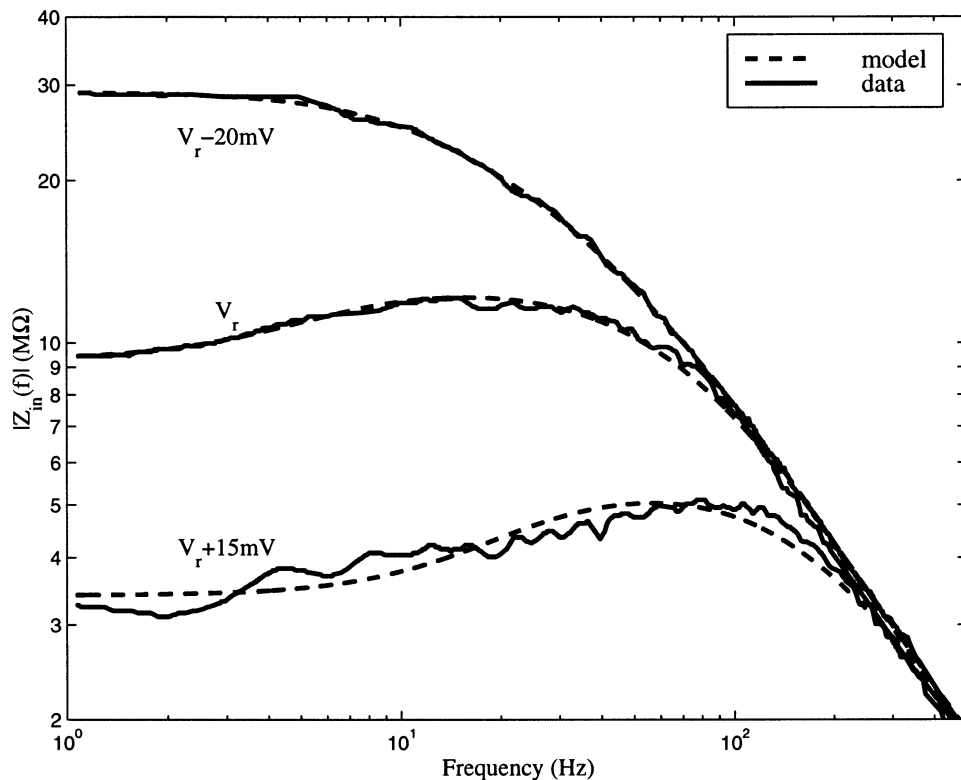
Acknowledgements

Fig. 9. Data from Juusola and Weckström (1993) and fits to input impedance of dark-adapted photoreceptor membrane as a function of frequency, when the membrane voltage is clamped at 20 mV below the dark resting potential (top), at dark resting potential (middle), and at 15 mV above dark resting potential (bottom).
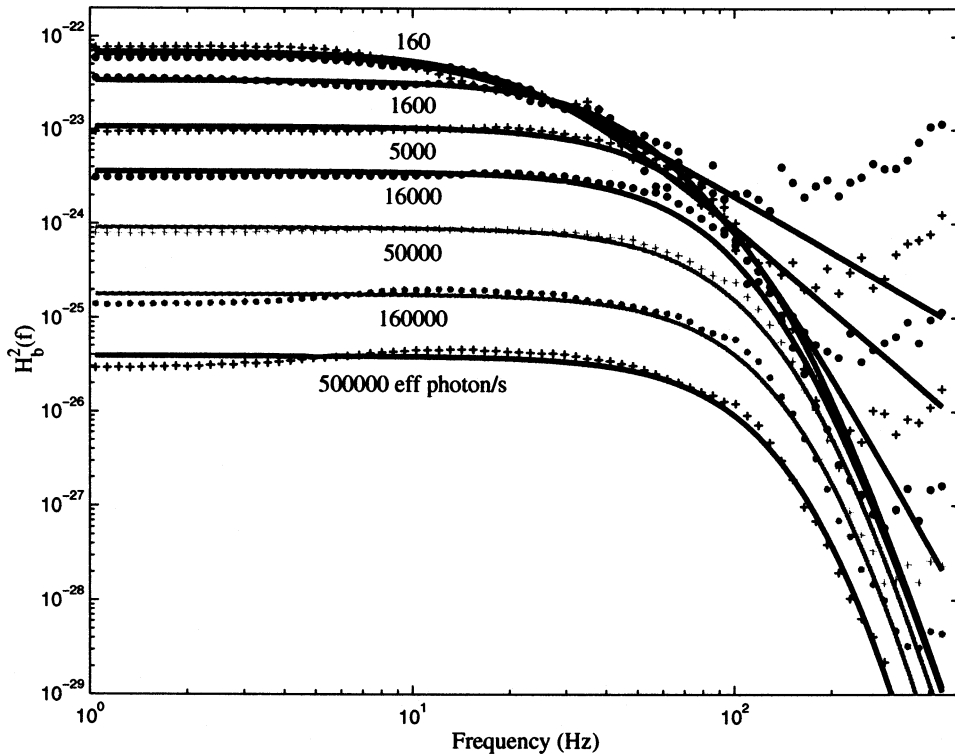
Fig. 10. Data scaled from Juusola et al. (1994) and model for biochemical transfer function $H_b^2(f)$ as a function of frequency for various light levels, from top to bottom corresponding to [160, 500, 1600, 5000, 16000, 50000, 160000, 500000] effective photons per s.

Goldberg for helping to make the paper more readable.

Appendix A. Model Parameters, Data Extraction and Estimation Procedures

Every modeling effort must rely on reliable experimental data for parameter extraction and model validation. In an ideal situation, the source of the data is a single experiment or experimental preparation that employs a single animal. Unfortunately, this ideal scenario rarely exists. To determine the parameters of our model, a rather diverse set of data was employed from different groups and in some instances even from different species. In an attempt to reconcile the discrepancies between the model and the data we employed multiple methods for extracting some of the model parameters.

In this section, we elaborate the procedures for estimating the parameters in our model. Table 1 gives descriptions, values, and citations for parameters and data that are taken directly from the literature. We extract numerical values for the data in published figures by scanning and processing using custom MATLAB® functions (Math Works, Inc., 1997). The positions of individual data points were obtained using template matching when possible and manually otherwise. Data representative of drawn lines were selected using thresholds and manipulated manually. The data were calibrated using axis marks from the ordinate and abscissa of the figure from which they were obtained. Numerical optimization was used to estimate parameters from the calibrated data. For data represented as a function of frequency f and voltage V, the optimizations minimized an objective function which was computed as the sum of the squared differences between the loga-

rithms of the data and model, $\Sigma_V\Sigma_f(\log(\text{DATA}(f,V)) - \log(\text{MODEL}(f,V)))^2$. We performed constrained optimization, using the Matlab function 'constr', to restrict the parameter space explored between 10 and 1000% of the starting values.

Membrane Impedance Parameters

We estimate parameters for the photoreceptor membrane using data representing the input impedance of the dark-adapted membrane when clamped at three different voltages, from Fig. 4b of Juusola and Weckström (1993). This data is shown in Fig. 9, alongside the curves computed with the theoretical model using parameters estimated from the sum-square-log optimization procedure described above. We model the dark adapted input impedance $Z_{in}(f)$ using the cable model of Fig. 2b, in the case of six coupled photoreceptor cells, with current entering only one of them (as the voltage clamp was applied to a single cell). The parallel conductances of Fig. 3 have been lumped into a single term, $g_m(V) = g_K(V) + g_{leak} + g_L(V(I))$, where the symbol I denotes dependence on the incident light intensity. We assume that the potassium conductance depends only on the membrane voltage V, the light-gated conductance depends on V through its dependence on the light intensity I, and the leakage conductance does not depend on V or I. We take starting values for the membrane resistance $R_m = 1/g_m$ and anatomical parameters (l_b, r_b, and SA_{rhab}) from van Hateren (1986). Values for the parameters that are not optimized (R, C_m, C_t, R_t, r_a, l_a, R_g, and R_b) are listed in Table 1.

We obtain values for the voltage-dependent quantities, $g_m(V)$, $g_n(V)$, and $L_n(V)$, at each of the three clamp voltages used in the experiments. We obtain a single value for each anatomical parameter l_b, r_b, and SA_{rhab}:

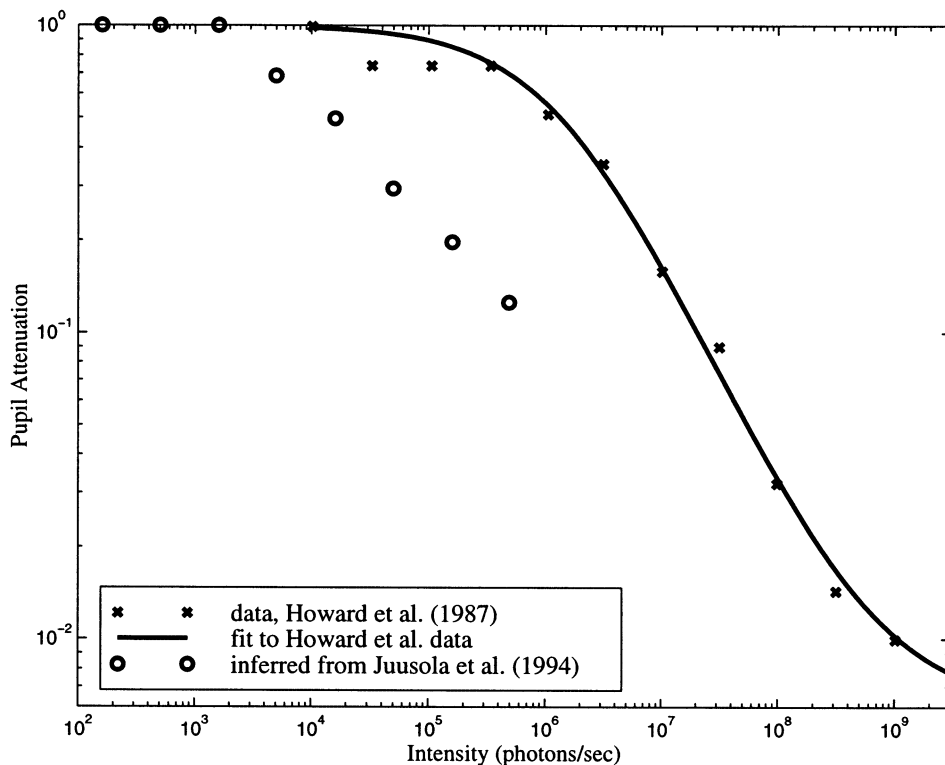Fig. 11. Pupillary attenuation as determined by Howard et al. (1987) ('x's) and as determined by fitting noise data of Juusola et al. (1994) ('o's). The solid line is our sigmoidal fit to the data of Howard et al. (1987).

$$\frac{1}{g_{\mathrm{m}}(V)} = \begin{bmatrix} 0.886 \\ 0.360 \\ 0.103 \end{bmatrix} \Omega\mathrm{m}^2,$$

$$\frac{1}{g_n(V)} = \begin{bmatrix} -1.43 \\ 0.615 \\ 0.132 \end{bmatrix} \Omega\mathrm{m}^2,$$

$$L_n(V) = \begin{bmatrix} -3.29 \\ 23.71 \\ 1.47 \end{bmatrix} \mathrm{mHm}^2,$$

$$\begin{bmatrix} l_{\mathrm{b}} = 114 \\ r_{\mathrm{b}} = 3.10 \\ SA_{\mathrm{rhab}} = 63.8 \end{bmatrix} \mu\mathrm{m}$$

We now make a few assumptions to estimate the remaining parameters for the photoreceptor membrane model of Fig. 3. The measurements of input impedance were performed in the dark-adapted membrane, and under these conditions, there is no conductance associated with the light-gated channels, i.e. $g_{\mathrm{L}}(V) = 0$. With a resting potential $V_{\mathrm{r}} = -60$ mV and the activation threshold for the potassium channels ≈ -75 mV (Weckström et al., 1991), there is no conductance associated with the potassium channels at the lowest clamped voltage, i.e. $g_{\mathrm{K}}(V_{\mathrm{r}} - 20\ \mathrm{mV}) = 0$. Under these two assumptions, the membrane leakage conductance g_{leak} is $g_{\mathrm{m}}(V_{\mathrm{r}} - 20\ \mathrm{mV})$. When the membrane is clamped at the two higher voltages, V_{r} and $V_{\mathrm{r}} + 15$ mV, the parallel conductance $g_{\mathrm{m}}(V)$ is attributed not only to leakage, which is assumed to be independent of voltage, but also to potassium channels, which are voltage-dependent. Using our estimate for g_{leak}, we can now estimate $g_{\mathrm{K}}(V)$, specifically $g_{\mathrm{K}}(V) = g_{\mathrm{m}}(V) - g_{\mathrm{leak}}$. The reversal potential for the leakage current E_{leak} is estimated from the reversal potential E_{K} for the potassium current (Weckström et al., 1991), the dark resting potential V_{r} (Weckström et al., 1991), and the estimated leakage and potassium conductances, g_{leak} and $g_{\mathrm{K}}(V_{\mathrm{r}})$.

Determining the potassium conductance at two voltages is the first step in estimating the potassium conductance and dynamical parameters and

the light-gated conductance over a range of voltages. From the conductance $g_{\mathrm{K}}(V)$ and dynamical parameters $g_n(V)$ and $L_n(V)$ for the potassium channels we estimate the channel activation parameters α, β, and ζ at the membrane voltages V_{r} and $V_{\mathrm{r}} + 15$ mV:

$$\alpha(V) = \frac{n_\infty}{\tau} = \frac{g_{\mathrm{K}}(V)}{N_{\mathrm{K}\gamma\mathrm{K}}} \frac{g_n(V)}{L_n(V)} \tag{A.1}$$

$$\beta(V) = \frac{1}{\tau} - \alpha = \left(1 - \frac{g_{\mathrm{K}}(V)}{N_{\mathrm{K}\gamma\mathrm{K}}}\right)\frac{g_n(V)}{L_n(V)} \tag{A.2}$$

$$\varsigma(V) = \frac{1}{L_n(V)}(V - E_{\mathrm{K}}) \tag{A.3}$$

We interpolate linearly to find activation parameters for the potassium channels at all other voltages, and we invert the above system of equations to estimate the potassium conductance and dynamical parameters as a function of voltage. We estimate the light-gated conductance at intermediate voltages from the reversal potentials of potassium (Weckström et al., 1991) and of the light-gated conductance (Hardie and Minke, 1993), from data representing the steady state membrane voltage as a function of incident light (Fig. 4a of Juusola et al., 1994), and from the leakage and potassium conductances and leakage reversal potential estimated above.

In the process of estimating parameters for our membrane impedance model, we also estimated most of the parameters for the ion channel noise model. The only remaining channel parameter is the total number of light-gated channels. We were unable to find an estimate for its value in our review of the literature. Values less than 2×10^4 result in unphysiological channel parameters (e.g. $n_\infty < 0$). The requirement for meaningful channel parameters provides only a lower bound for N_{L}. This uncertainty was exploited by allowing N_{L} to be a free parameter in fitting the noise data described below. When the noise data was not fit explicitly we assume that $N_{\mathrm{L}} = 10^6$. We take the latter value to be a reasonable guess, as there are 10^5 microvilli and 10^8 rhodopsin molecules in those microvilli. One of the putative light-gated channels is localized along the base of the microvilli (Pollock et al., 1995), so the number of

light-gated channels should be between 10^5 and 10^8. The latter assumption does not have a strong effect on the predicted membrane noise, although the predicted noise decreases slightly with increasing N_L.

Biochemical Cascade Parameters

We estimate parameters for the biochemical cascade, $h_b(I)$, $t_b(I)$, and $n_b(I)$, using data from Fig. 7 of Juusola et al. (1994), which represents the measured transfer function from effective photon rate to membrane voltage at eight background light levels. This data was scaled by the transfer functions corresponding to the optical attenuation ($H_o(f)$, Eq. (5)), the channels ($H_c(f)$, Eq. (10)), and the membrane impedance ($H_m(f) = |Z_{in}(f)|$). The scaled data reflects the biochemical cascade portion of the transfer function. Fig. 10 shows the model (solid lines) and scaled physiological data (symbols) at the eight light levels. Parameters for the optical transfer function H_o are determined either from a fit to the data of Howard et al. (1987) or from a fit of predicted noise with measured noise as described below. Parameters for the channel transfer function H_c are the steady state membrane voltage at the eight background light levels, given by Fig. 4a of Juusola et al. (1994) and the reversal potential for the light-gated conductance E_L (Hardie and Minke, 1993). Parameters for the membrane impedance transfer function $H_m(f)$ were estimated as discussed above. We employ the input impedance rather than the transfer impedance because the voltage data was measured at the cell body. We model the input impedance $Z_{in}(f)$ using the cable model of Fig. 2b, in the case of six coupled photoreceptor cells, with current entering all six of them (as the input light was applied to all six cells).

The model for the frequency response of a gamma function (Eq. (9)) was matched to the data using numerical optimization as described earlier, with further constraints imposed to restrict each biochemical cascade parameter ($h_b(I)$, $t_b(I)$, and $n_b(I)$) to vary monotonically with the intensity and to restrict the implied channel parameters to be plausible (i.e. $0 < n_\infty < 1$). The data at higher frequencies from Fig. 7 of Juusola et al. (1994) was ignored because it appeared to be

unreliable above cutoff frequencies ranging from 130 to 350 Hz. The parameters for the membrane impedance are used to fit the biochemical cascade, so the impedance and biochemical cascade parameters were subsequently optimized together, using constrained optimization to restrict the parameter space explored between 50 and 200% of the earlier optimized values. This joint optimization did not change the membrane impedance parameters significantly.

Eight values are obtained and listed below for each of the parameters, $h_b(I)$, $t_b(I)$, and $n_b(I)$, at the background light levels $I = [160, 500, 1600, 5000, 16000, 50000, 160000, 500000]$ effective photons per s:

$$h_b(I) = \begin{bmatrix} 8.0975 \\ 8.2449 \\ 5.7855 \\ 3.2701 \\ 1.8997 \\ 0.9500 \\ 0.4242 \\ 0.1979 \end{bmatrix} \text{pS/Rh,}$$

$$t_b(I) = \begin{bmatrix} 8.9024 \\ 6.5192 \\ 2.3889 \\ 1.2590 \\ 1.1276 \\ 0.9302 \\ 0.7859 \\ 0.7199 \end{bmatrix} \text{ms,} \quad n_b(I) = \begin{bmatrix} 0.0084 \\ 0.5041 \\ 2.1654 \\ 4.3509 \\ 4.3852 \\ 4.9743 \\ 5.7908 \\ 6.7294 \end{bmatrix}$$

A second set of parameters for the biochemical cascade model was obtained using data from Fig. 7a of Juusola et al. (1995). The results were similar to those listed above. The biochemical cascade parameters at intermediate light levels were determined by interpolating the logarithms of the parameters linearly with the logarithm of the light level I.

Optical Attenuation Parameters

We estimate optical attenuation from an empir-

ical fit to the data of Howard et al. (1987), as discussed in Section 2.2, and obtain parameters $p_1 = -1.90$, $p_2 = -6.12$, and $p_3 = 6.15 \times 10^{-3}$. The values used for the pupillary attenuation strongly affect the noise predicted by our model. While Fig. 4 shows some qualitative agreement between measured and predicted membrane voltage noise, this agreement can be improved quantitatively by estimating parameters using the membrane noise data from Fig. 5c of Juusola et al. (1994). We estimate the pupillary attenuation $C_o(I)$ and the number of light-gated channels N_L using numerical optimization as described above, with further constraints imposed to restrict the attenuation to vary monotonically with the intensity, to take values between 0 and 1, and to restrict the implied channel parameters to be plausible (i.e. $0 < n_\infty < 1$). The data at frequencies below 4.5 Hz was ignored, since none of the noise sources in our model can account for the excess low frequency noise. We obtain the number of light-gated channels $N_L = 3.4 \times 10^4$, and eight values for the pupillary attenuation, $C_o(I)$, as a function of light level I:

$$C_o(I) =$$

$$[1.0 \ \ 1.0 \ \ 1.0 \ \ 1.0 \ \ 0.687 \ \ 0.497 \ \ 0.296 \ \ 0.197 \ \ 0.126] \tag{A.4}$$

The pupillary attenuation estimated by our numerical optimization is shown as circles in Fig. 11 and is much stronger than that determined by Howard et al. (1987) for the corresponding light levels.

Using our values for the pupillary attenuation (Eq. (A.4)), the membrane voltage noise predicted by our model shows quantitative agreement with the measured noise, in contrast with the predicted membrane voltage noise shown in Fig. 4 that employs our empirical fit to the pupillary attenuation data from Howard et al. (1987). The left panel of Fig. 5 shows measured noise data from Juusola et al. (1994), and the right panel shows the results of our model, using the parameters for membrane impedance, biochemical cascade, and our values for the estimated pupillary attenuation (given in Eq. (A.4)).

References

Abshire P., Andreou A.G., 1998. Relating information capacity to a biophysical model of the blowfly retina. Technical Report JHU/ECE-98-13, Johns Hopkins Univ., Dept. of Elec. and Comp. Eng., Baltimore, MD, 1998.

Abshire P., Andreou A.G., 1999a. Information capacity of the blowfly retina. In: Proceedings of the 33rd Conference on Information Sciences and Systems, Baltimore, MD, March 1999.

Abshire P., Andreou A.G., 1999b. Relating information capacity to a biophysical model for blowfly retina. In: Proceedings of the 1999 International Joint Conference on Neural Networks, Washington, DC, July 1999.

Abshire P., Andreou, A.G., 2000a. A comparative study of information capacity for biophysical and silicon photoreceptors. In: Proceedings, ISCAS 2000, Geneva.

Abshire P., Andreou, A.G., 2000b. Relating information capacity to a biophysical model for blowfly photoreceptors. Neurocomputing, 32–33, 9–16.

Atick, Joseph J., 1992. Could information theory provide an ecological theory of sensory processing? Network 3, 213–251.

Attneave, Fred, 1954. Some informational aspects of visual perception. Psychol. Rev. 61 (3), 183–193.

Barlow, B.A., 1961. Possible principles underlying the transformation of sensory messages. In: Rosenblith, W.A. (Ed.), Sensory Communication. MIT Press, Cambridge, MA, pp. 217–234.

Bialek, W., 1987. Physical limits to sensation and perception. Ann. Rev. Biophys. Biophys. Chem. 16, 455–478.

Birge, R.R., Barlow, R.B., 1995. On the molecular origins of thermal noise in vertebrate and invertebrate photoreceptors. Biophys. Chem. 55, 115–126.

Braitenberg, V., 1967. Patterns of projection in visual system of fly. I. Retina-lamina projections. Exp. Brain Res. 3, 3.

Buračas, Giedrius T., Zador, Anthony M., DeWeese, Michael R., Albright, Thomas D., 1998. Efficient discrimination of temporal patterns by motion-sensitive neurons in primate visual cortex. Neuron 20, 959–969.

Cover, Thomas M., Thomas, Joy A., 1991. Elements of Information Theory. Wiley, New York.

de Ruyter van Steveninck, R.R., Laughlin, S.B., 1996. The rate of information transfer at graded-potential synapses. Nature 379, 642–645.

DeFelice, L.J., 1981. Introduction to Membrane Noise. Plenum Press, New York.

Eckert, Hendrik, Bishop, Lewis G., 1975. Nonlinear dynamic transfer characteristics of cells in the peripheral visual pathway of flies. Part I: The retinula cells. Biol. Cyberbetics 17, 1–6.

Eckhorn Reinhard, Pöpel Bertram, 1974. Rigorous and extended application of information theory to the afferent visual system of the cat. I. Basic concepts, and II. Experimental results. Kybernetik, 16–17:191–200, 7–17.

French, A.S., Järvilehto, M., 1978. The transmission of information by first and second order neurons in the fly visual system. J. Comp. Physiol. A 126, 87–96.

French, A.S., Korenberg, M.J., Jirvilehto, M., Kouvalainen, E., Juusola, M., Weckström, M., 1993. The dynamic non-linear behavior of fly photoreceptors evoked by a wide range of light intensities. Biophys. J. 65, 832–839.

Hardie, Roger C., 1979. Electrophysiological analysis of fly retina. I: Comparative properties of R1-6 and R7 and 8. J. Comp. Physiol. A 129, 19–33.

Hardie, R.C., Minke, B., 1993. Novel Ca^{2+} channels underlying transduction in Drosophila photoreceptors: implications for phosphoinositide-mediated Ca^{2+} mobilization. TINS 16 (9), 371–376.

Hardie, R.C., Minke, B., 1994. Spontaneous activation of light-sensitive channels in Drosophila photoreceptors. J. Gen. Physiol. 103, 389–407.

Hochstrate, P., Hamdorf, K., 1990. Microvillar components of light adaptation in blowflies. J. Gen. Physiol. 95, 891–910.

Howard, J., Blakeslee, Barbara, Laughlin, S.B., 1987. The intracellular pupil mechanism and photoreceptor signal:noise ratios in the fly *Lucilia cuprina*. Proc. R. Soc. Lond. B 231, 415–435.

Johnston, D., Wu, S.M., 1997. Foundations of Cellular Neurophysiology. MIT Press, Cambridge, MA.

Juusola, M., 1993. Linear and non-linear contrast coding in light-adapted blowfly photoreceptors. J. Comp. Physiol. A 172, 511–521.

Juusola, Mikko, Weckström, Matti, 1993. Band-pass filtering by voltage-dependent membrane in an insect photoreceptor. Neurosci. Lett. 154, 84–88.

Juusola, M., Kouvalainen, E., Jarvilehto, M., Weckström, M., 1994. Contrast gain, signal-to-noise ratio, and linearity in light-adapted blowfly photoreceptors. J. Gen. Physiol. 104, 593–621.

Juusola, M., Uusitalo, R.O., Weckström, M., 1995. Transfer of graded potentials at the photoreceptorinterneuron synapse. J. Gen. Physiol. 105, 117–148.

Laughlin, Simon B., 1994. Matching coding, circuits, cells, and molecules to signals: general principles of retina design in the fly's eye. Progr. Retinal Eye Res. 13, 165–196.

Leutscher-Hazelhoff, J.T., Kuiper, J.W., 1964. Responses of the blowfly *Calliphora erythrocephala* to light flashes and to sinusoidally modulated light. Doc. Ophthalmol. 18, 275–284.

Levy, William B., Baxter, Robert A., 1996. Energy efficient neural codes. Neural Comput. 8, 531–543.

Lillywhite, P.G., 1977. Single photon signals and transduction in an insect eye. J. Comp. Physiol. A 122, 189–200.

Linsker Ralph, 1986. From basic network principles to neural architecture: Emergence of spatial-opponent cells, Emergence of orientation-selective cells, and Emergence of orientation columns. Proc. Natl. Acad. Sci. USA, 83:7508–7512, 8390–8394, 8779–8783.

MacKay, Donald M., McCulloch, Warren S., 1952. The limiting information capacity of a neuronal link. Bull. Math. Phys. 14, 127–135.

Manwani Amit, Koch Christof, 1999. Detecting and estimating signals in noisy cable structures: I. Neuronal noise sources, and II. Information theoretical analysis. Neural Computation, 11:1797–1829, 1831–1873.

MATLAB is a registered trademark of The MathWorks, Inc. for MATLAB product information, please contact The MathWorks, Inc., J Apple Hill Drive, Natick, MA 01760-2098 USA. Tel.: 508-647-7000; fax: 508-647-7001, E-mail: info@mathworks.com, Web: www.mathworks.com.

Pollock, John A., Assaf, Arnon, Peretz, Asher, Nichols, Charles D., Mojet, Mart H., Hardie, Roger C., Minke, Baruch, 1995. TRP, a protein essential for inositide-mediated Ca^{2+} influx is localized adjacent to the calcium stores in Drosophila photoreceptors. J. Neurosci. 15, 3747–3760.

Reuss, Helmut, Mojet, Mart H., Chyb, Sylwester, Hardie, Roger C., 1997. In vivo analysis of the Drosophila light-sensitive channels, TRP and TRPL. Neuron 19, 1249–1259.

Rieke, Fred, Warland, David, van Steveninck, Rob de Ruyter, Bialek, William, 1997. Spikes: Exploring the Neural Code. MIT Press, Cambridge, MA.

Shannon C.E., 1948. A mathematical theory of communication. Bell Syst. Tech. J., 27:379–423, 623–656.

Shannon Claude E., 1949. Communication in the presence of noise. Proceedings of the L. R. E., 37:10–21, Jan 1949.

Shaw, S.R., 1984. Asymmetric distributions of gap-junctions amongst identified photoreceptor axons of Lucilia cuprina (Diptera). J. Cell. Sci. 66 (Mar), 65–80.

Stein, Richard B., 1967. The information capacity of nerve cells using a frequency code. Biophys. J. 7, 797–826.

Teich, M.C., Saleh, B.E.A., 1982. Effects of random deletion and additive noise on bunched and anti-bunched photon statistics. Opt. Lett. 7 (8), 365–367.

Theunissen, Frédéric E., Miller, John P., 1991. Representation of sensory information in the cricket cercal sensory system. II. Information theoretic calculation of system accuracy and optimal tuning-curve widths of four primary interneurons. J. Neurophysiol. 66 (5), 1690–1703.

van Hateren, J.H., 1986. Electrical coupling of neuro-ommatidial photoreceptor cells in the blowfly. J. Comp. Physiol. A 158, 795–811.

Weckström, M., Hardie, R.C., Laughlin, S.B., 1991. Voltage-activated potassium channels in blowfly photoreceptors and their role in light adaptation. J. Physiol. 440, 635–657.

Weckström, M., Juusola, M., Laughlin, S.B., 1992. Presynaptic enhancement of signal transients in photoreceptor terminals in the compound eye. Proc. R. Soc. Lond. B250, 83–89.

Wong, F., Knight, B.W., 1980. Adapting-bump model for eccentric cells of Limulus. J. Gen. Physiol. 76, 539–557.

Wong, F., Knight, B.W., Dodge, F.A., 1980. Dispersion of latencies in photoreceptors of Limulus and the adapting-bump model. J. Gen. Physiol. 76, 517–537.

Wong, Fulton, Knight, Bruce W., Dodge, Frederick A., 1982. Adapting-bump model for ventral photoreceptors of Limulus. J. Gen. Physiol. 79, 1089–1113.